

Evaluating the electromigration effect on mechanical performance degradation of aluminum interconnection wires

A nanoindentation test with molecular dynamics simulation study

Feng, Shuo; Du, Leiming; Cui, Zhen; Zhu, Xi; Fan, Xuejun; Zhang, Guoqi; Fan, Jiajie

DOI

[10.1016/j.apsusc.2024.160992](https://doi.org/10.1016/j.apsusc.2024.160992)

Publication date

2024

Document Version

Final published version

Published in

Applied Surface Science

Citation (APA)

Feng, S., Du, L., Cui, Z., Zhu, X., Fan, X., Zhang, G., & Fan, J. (2024). Evaluating the electromigration effect on mechanical performance degradation of aluminum interconnection wires: A nanoindentation test with molecular dynamics simulation study. *Applied Surface Science*, 676, Article 160992. <https://doi.org/10.1016/j.apsusc.2024.160992>

Important note

To cite this publication, please use the final published version (if applicable). Please check the document version above.

Copyright

Other than for strictly personal use, it is not permitted to download, forward or distribute the text or part of it, without the consent of the author(s) and/or copyright holder(s), unless the work is under an open content license such as Creative Commons.

Takedown policy

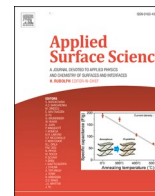
Please contact us and provide details if you believe this document breaches copyrights. We will remove access to the work immediately and investigate your claim.

Green Open Access added to TU Delft Institutional Repository

'You share, we take care!' - Taverne project

<https://www.openaccess.nl/en/you-share-we-take-care>

Otherwise as indicated in the copyright section: the publisher is the copyright holder of this work and the author uses the Dutch legislation to make this work public.



Full Length Article

Evaluating the electromigration effect on mechanical performance degradation of aluminum interconnection wires: A nanoindentation test with molecular dynamics simulation study

Shuo Feng^a, Leiming Du^b, Zhen Cui^b, Xi Zhu^c, Xuejun Fan^d, Guoqi Zhang^b, Jiajie Fan^{a,b,c,*}

^a Shanghai Engineering Technology Research Center for SiC Power Device, Academy for Engineering & Technology, Fudan University, Shanghai 200433, China

^b EEMCS Faculty, Delft University of Technology, Delft 2628, the Netherlands

^c Research Institute of Fudan University in Ningbo, Ningbo 315336, China

^d Department of Mechanical Engineering, Lamar University, PO Box 10028, Beaumont, TX 77710, USA

ARTICLE INFO

Keywords:

- A. Aluminum interconnects
- B. Electromigration
- C. Nanoindentation
- D. Mechanical property

ABSTRACT

Electromigration (EM) is a crucial failure mode in Aluminum (Al) interconnection wires those are widely used in high density semiconductor packaging. This study systematically investigated the influence of EM on the mechanical properties of Al interconnects via nanoindentation experiments and molecular dynamics (MD) simulations. The results are list as follows. (1) The indentation depth gradually increases with the increase in indentation load, resulting in a gradual increase and stabilization of the Young's modulus and hardness of the structure. Within a specific range, the influence of the loading rate on the indentation depth and mechanical properties is relatively small. (2) The region where Young's modulus of the interconnect decreases correlates with the location where EM-induced voids initiate. EM-induced voids have a direct impact on the material's mechanical properties, particularly the decrease in Young's modulus. (3) These EM-induced voids affect the nucleation and formation of dislocations. With the increase in void concentration and indentation depth, The generation and slip of dislocations increase as the void concentration and indentation depth increase, leading to a decrease in the material's mechanical properties over time. This comprehensive findings expand the knowledge on mechanical behavior degradation of Al interconnects when EM failure occurs, providing a scientific basis for designing and optimizing high density semiconductor packaging.

1. Introduction

Electromigration (EM), a phenomenon characterized by the directed motion of metal atoms under the influence of an electric current, is crucial in microelectronics and semiconductor technology [1,2]. The continuous downscaling of integrated circuits and the escalating demand for improved device performance have intensified the challenges associated with EM-induced failures [3,4]. Aluminum (Al), widely employed as an interconnect material due to its favorable electrical conductivity and processability, is particularly susceptible to EM-induced degradation [5,6]. Under the influence of current, electron wind drives the migration of Al atoms within an interconnect, generating vacancies in the structure, manifesting macroscopically as the formation of voids and hillocks [7,8]. When vacancies are generated, the surrounding atoms tend to relax. Consequently, the volume occupied by

vacancies (Ω_v) becomes a fraction of the atomic volume (Ω_a), and the accumulation of vacancy concentration leads to the shrinkage of the local trading volume. Conversely, the depletion of the vacancy concentration results in the expansion of the local volume [9,10]. The generated structural changes induce mechanical stress in the material, influencing the mechanical performance of the interconnect. This threatens its integrity and functionality, ultimately affecting the overall performance and lifespan of microelectronic devices [11–13]. However, existing research on the factors affecting the mechanical properties of interconnects mainly focuses on thermal aging, and the failure factor of EM is not comprehensive. Thus, a systematic approach to fill this gap needs to be developed.

Nanomechanical testing, particularly nanoindentation, has emerged as a powerful and precise tool for probing the mechanical properties of materials at the nanoscale [14,15]. The technique involves applying

* Corresponding author.

E-mail address: jiajie_fan@fudan.edu.cn (J. Fan).

<https://doi.org/10.1016/j.apsusc.2024.160992>

Received 10 May 2024; Received in revised form 31 July 2024; Accepted 14 August 2024

Available online 20 August 2024

0169-4332/© 2024 Elsevier B.V. All rights are reserved, including those for text and data mining, AI training, and similar technologies.

controlled forces to a nanoscale indenter and measuring the resulting material response, offering valuable insights into hardness, elasticity, and deformation behavior [14]. Nanoindentation has extensive applications in materials science, providing a nuanced understanding of material performance, especially in small-scale structures and devices [16,17]. As a complement to experimental studies, molecular dynamics (MD) simulations have evolved as a complementary approach for elucidating the atomic-scale mechanisms governing material behavior [18–20]. By numerically solving Newton’s equations of motion for a system of interacting atoms, MD simulations enable researchers to explore the dynamic evolution of materials under various conditions, uncovering fundamental insights into their structural changes, mechanical responses, and failure mechanisms [21,22].

The combination of nanoindentation experiments with MD simulations will allow the comprehensive investigation of the mechanical properties and deformation mechanisms of materials at the nanoscale [23,24]. Wang *et al.* employed atomistic simulations in conjunction with nanoindentation experiments to investigate the deformation behavior of single-crystal silicon and polycrystalline silicon materials. They unveiled phenomena such as nanoindentation-induced phase transitions and grain size effects. This approach bridges experimental and computational perspectives and facilitates a more holistic understanding of material behavior under diverse loading conditions and environmental factors. Generally, aluminum (Al) is considered a very suitable material for studying the mechanical properties of face-centered cubic (FCC) metals using MD. Jiao *et al.* [25] used simulations to understand prismatic dislocation loop formation with a rigid diamond indenter to investigate Al (100). The force–displacement curve analysis revealed crystal defect evolution. Based on the vacancy clustering mechanism and the formation mechanism of Frank loops in stacking fault tetrahedra (SFT), Kumar Panda *et al.* [26] simulated atomic-scale processes using MD. They provided insights into the stepwise evolution process from vacancy clusters and dislocation loops to SFT. The phenomenon of EM-induced voids in interconnects is attributed to the accumulation of vacancies within the microscopic internal structure. In this study, to simulate the effects of EM, we artificially introduced a specific concentration of vacancies into the MD model and analyzed it in conjunction with nanoindentation.

This study aimed to comprehensively understand the effect of EM on the mechanical properties of Al interconnects. By combining nanoindentation experiments with MD simulations, we studied the intricate interplay between EM, mechanical properties, and deformation mechanisms in Al interconnects. The influence of indentation depth and loading rate on material performance was examined by conducting indentation experiments on Al interconnects with different EM-induced damage. The study researched the effect of EM on Young’s modulus and the hardness of the interconnects. MD simulations were employed to

simulate changes in indentation performance with different void concentrations to gain a deeper understanding of this phenomenon. This comprehensive investigation aimed to elucidate the microscopic mechanisms and macroscopic manifestations of EM on the material properties of Al interconnects.

2. Experimental details

This section provides details about the sample preparation and nanoindentation experimental setups.

2.1. Sample preparation

Fig. 1(a) shows the stacking layer structure of the EM test sample. The sample fabrication began with growing 200-nm-thick SiO₂ via thermal oxidation on a silicon wafer as an etch stop layer and a thermally isolated layer. Then, a 300-nm-thick titanium nitride (TiN) layer was deposited on the SiO₂ layer by sputtering. In this process, TiN was formed in the vacuum chamber by the reaction between reactive gas (N₂) and vapor-phase titanium. It is noted that an oxidation layer is easily formed on the surface of the TiN layer, even at room temperature (25 °C). Thus, a hot sputter etch (HSE) process was used to remove the oxide layer on TiN. Subsequently, a 200-nm-thick Al layer was deposited on TiN using reactive sputtering at 300 °C. Then, the required standard wafer-level electromigration acceleration test (SWEAT) structure [27], where a narrow Al line was connected to two large pads on both sides (see Fig. 1(b)), was obtained using wet etching. Finally, samples were annealed at 450 °C for 30 min in a vacuum chamber to stabilize the microstructure of the Al lines [10].

Fig. 1(c) shows a schematic of the accelerated EM test setup in this study. This experimental setup includes a Nextron MPS-CHH microprobe chamber (Busan City, Korea) with a ceramic chuck, a temperature controller, a source measure unit (SMU, Keithley 2611b) and an optical microscope (AOSVI HD228S). To perform the electromigration test, the test chip was placed at the center of the microprobe chamber firstly. Then, four probe needles with 20 μm diameter rhodium tips were connected to the metal pad on the chip for power supply and electrical resistance measurement. Meanwhile, a temperature controller which was placed under the ceramic chuck was used to hold the desired temperature at a specified value. The temperature was capable of being raised from 50 to 500 °C in this study. Moreover, the optical microscope were employed to locate the Al interconnect and observe the EM-induced void evolution.

To investigate the effect of EM-induced voids on the mechanical properties of Al interconnect, we conducted EM experiments on two different-sized Al interconnect structures (5 μm × 800 μm / 15 μm × 1105 μm). The experiments were conducted at 25 °C, with a current

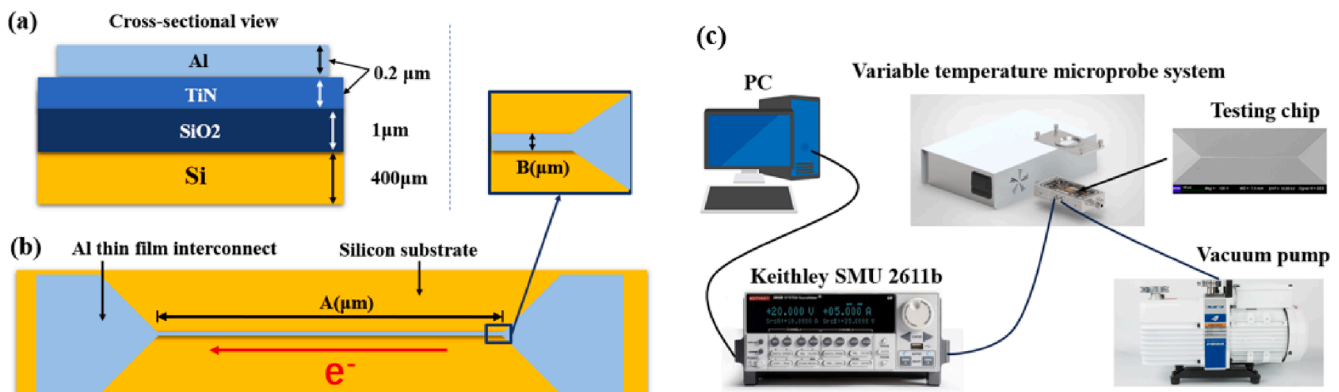


Fig. 1. (a) Illustration of the stacking layer of the Al interconnect sample. (b) Scanning electron microscopy (SEM) image of the Al interconnect structure. (c) Accelerated EM test setup.

density of 3 MA/cm². The applied current was maintained for 20 and 30 h in both structures, respectively.

2.2. Nanoindentation setup

The nanoindentation experiments were conducted at room temperature by using a KLA-iNano® nanoindenter (California, USA), which can perform various nanomechanical tests on materials, including nanoindentation, hardness, scratch, and general nanoscale testing. This equipment provides a wide dynamic measurement range for force and displacement, enabling precise and repeatable testing of materials ranging from soft polymers to metals.

In this research, a Berkovich tip was applied for the nanoindentation tests. Before the test, the test chip was placed on the stage. Subsequently, the sample surface was observed using an optical microscope to choose the indentation position. Then, the load rate and the maximum load value for indentation were set, and the indenter automatically conducted the nanoindentation experiment according to the configured conditions under the controlled system. Throughout the nanoindentation process, a load sensor with a resolution of 50 nN and a displacement sensor with a resolution of 0.01 nm provided real-time and high-precision recording of changes in load and displacement during the experiment. The continuous stiffness measurement (CSM) method was utilized to perform nanoindentation tests on the sample. The indenter used in the nanoindentation test had a conical shape with a radius of 20 nm.

2.3. Principles of nanoindentation

The hardness and Young's modulus of the compressed material can be calculated using the load–displacement curve. The classic method proposed by Oliver and Pharr in 1992, also known as the O&P method, has been widely adopted [28]. The O&P method characterizes the relationship between force and displacement during the unloading segment, approximately following the exponential function form:

$$P = a(h - h_f)^b, \quad (1)$$

where h represents the total displacement, and a , b , and h_f are determined through the least squares fitting method.

According to the Hertzian contact theory [29], the relationship between the applied load (P) and the indentation depth of the indenter (h) can be described by the formula of Hertzian contact theory:

$$P = \frac{4}{3} E \times r^{1/2} \times h^{3/2}, \quad (2)$$

where E represents the Young's modulus of the material being indented, and r denotes the radius of the indenter tip.

Hardness is a measure of the material's resistance to deformation, representing the maximum load it can withstand on the projected area of the indentation. The calculation formula is as follows:

$$H = \frac{P_{Max}}{A(h)}, \quad (3)$$

where $A(h)$ represents the projected contact area of the indenter. For the Berkovich indenter,

$$A(h) = 0.75 \bullet \tan(\theta) \bullet h^2, \quad (4)$$

where θ is the half-angle of the Berkovich indenter.

The formula for calculating Young's modulus E is as follows:

$$\frac{1}{E_r} = \frac{(1 - \nu^2)}{E} + \frac{(1 - \nu_i^2)}{E_i} \quad (5)$$

E , ν , E_i , and ν_i represent Young's modulus and Poisson's ratio (ν) of the test material and the indenter, respectively. The indenter material used

in our experiment was diamond, with an elastic modulus of $E_i = 1200$ GPa and Poisson's ratio of $\nu_i = 0.07$. The equivalent elastic modulus E_r can be determined from the following formula:

$$E_r = \frac{\sqrt{\pi}}{2\beta} \frac{S}{\sqrt{A(h_c)}} \quad (6)$$

where β is the geometric constant associated with the indenter. For a Berkovich indenter, $\beta = 1.034$.

3. Analysis of experimental results

3.1. Mechanical properties of Al interconnect before EM test

In this section, we investigated the influence of the indentation load and loading rate on the mechanical properties of Al interconnect before EM test (0 h). Initially, we obtained the load–displacement curves under different load conditions (10–50 mN) by setting the indentation loading rate at 0.5 mN/s. Indentation positions were chosen at the middle and both ends of the interconnect for comparison to ensure uniformity of the samples. As shown in Fig. 2, the P – h curves for different indentation depths overlap during the elastic loading stage. In the unloading phase, these curves exhibit similar characteristics. As the indenter moved upward, the load gradually diminished until it reached zero. Even after the complete disengagement of the indenter from the Al interconnect, the nanoindentation depth did not decrease to 0, indicating that permanent plastic deformation occurs in the material after nanoindentation tests.

Subsequently, the P – h curves under various loading rates were obtained by increasing the load rate from 0.1 to 0.5 mN/s while maintaining the current indentation load of 10 mN. The depth of the indentations was minimally affected by the loading rate while the indentation load was constant as shown in Fig. 3, and the morphology of the indentations did not differ significantly. Then, a nanoindentation scan (20 × 20) was performed on the Al interconnect under loading conditions of 10 mN and 0.2 mN/s to measure the average Young's modulus and hardness. Fig. 4c and d present the distribution of Young's modulus and hardness, respectively. The average Young's modulus (E^*) was 181.3 GPa, and the average hardness was 3.6 GPa. Afterwards, atomic force microscopy (AFM) was used to scan the sample's surface and measure the localized deformation to produce high-resolution topographic images. Results show that the measured indentation depth was approximately 400 nm, as shown in Fig. 4b.

According to Hertzian contact theory [29], we calculated Young's modulus and hardness of the P – h curves under different indentation loads and loading rates. As shown in Fig. 5a, Young's modulus and hardness increased with the indentation load increased from 10 to 20 mN, and then stabilised when the load increased from 20 to 50 mN. The hardness and Young's modulus measured at smaller indentation depths may be underestimated. This is caused by the commonly observed Indentation Size Effect (ISE) in nanoindentation technology. At smaller indentation depths, the measurement results are more significantly influenced by the material's microstructural characteristics, such as grain size and dislocation density. As the applied load and indentation depth increase, the influence of these microstructural characteristics gradually diminishes, and the measurement results become more stable. As shown in Fig. 5b, the loading rate has only a limited effect on Young's modulus and hardness, which only show a very limited increase as the loading rate increases.

3.2. Effect of EM on the mechanical properties of Al interconnect

To evaluate the effect of EM on the mechanical properties, we conducted nanoindentation experiments on the Al interconnects subjected to EM tests. In this section, EM tests of 20 h and 30 h are conducted to test different sizes of Al interconnects. High-resolution SEM scans were performed to observe the surface morphology and microstructure of the

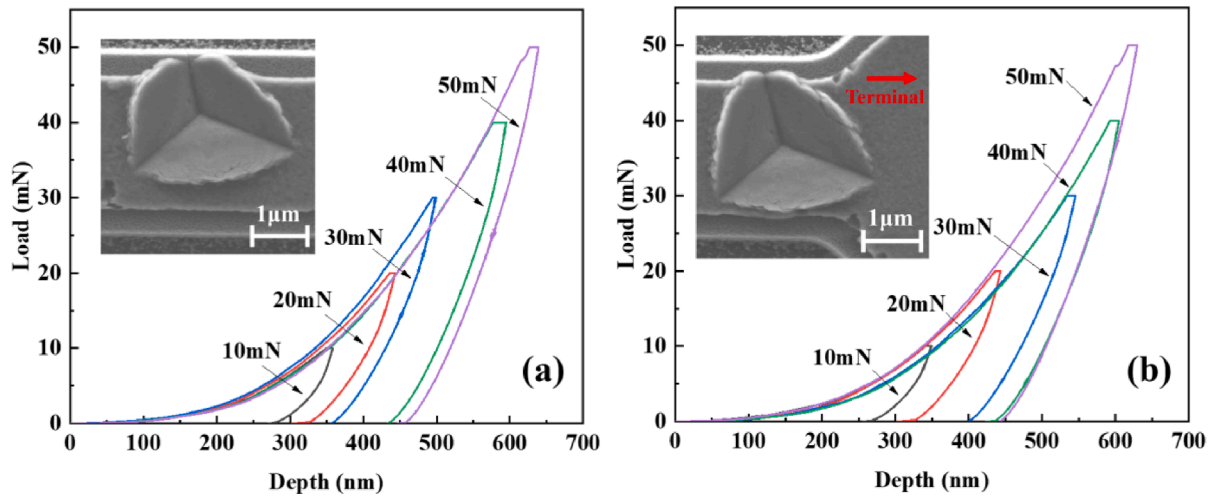


Fig. 2. P - h curves of the Al interconnect under different loads: (a) at the middle location of Al interconnect; (b) at the end side of the Al interconnect.

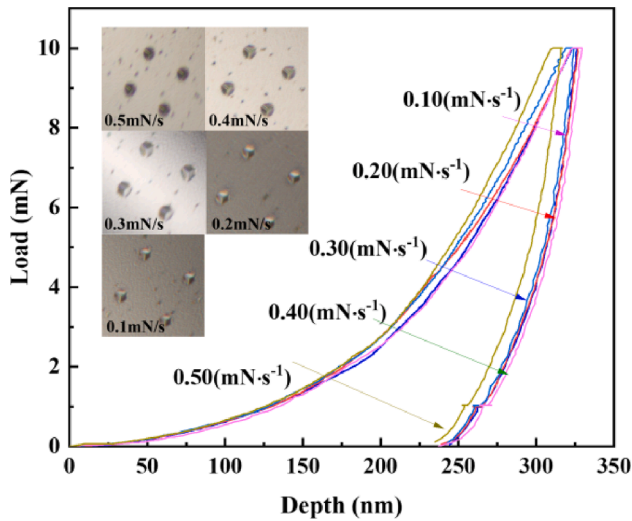


Fig. 3. P - h curves of the interconnect under different loading rates.

Al interconnect, as illustrated in Fig. 6. As the duration of the electrical current increases, the current density within the interconnect structure may cause metal atoms to migrate locally, leading to void formation. These voids may manifest as microscopic pores or depressions on the interconnect surface. Additionally, EM may result in changes in the crystal structure, including the rearrangement of grains and the formation of dislocations [30–32].

The structural changes in the interconnect may lead to variations in material mechanical properties. Nanoindentation experiments were conducted to measure Young's modulus of the Al interconnects after different EM duration, providing insights into the effect of EM on its mechanical properties. As shown in Fig. 7, Young's modulus of the Al interconnects significantly decreased with an increase in the applied current duration, particularly in the structural segment ($x/L = 0.5$ – 0.65) coinciding with the initiation region of interconnect voids, especially during the initial 0–20 h. This decreasing trend in mechanical performance is likely associated with void generation. As EM progressed, the interconnect resistance sharply increased, leading to the formation of local discontinuities. Notably, during the 20–30 h, the decrease in the material's Young's modulus was relatively small. This observation may be attributed to the stabilization of void generation induced by EM and a gradual reduction in the effect of local discontinuities on EM.

4. Simulation methodology and results

In this section, we used the MD simulations to analyze the EM effect on mechanical performance degradation of Al interconnection wires with simplified single-crystal model at the atomic scale.

4.1. Basic modeling equations

In a system consisting of a total of n lattice sites with n_v vacancies, the overall volume of the system is the combined volume occupied by both atoms and vacancies:

$$V = n_a \Omega_a + n_v \Omega_v \quad (7)$$

where n_a represents the number of atoms, and $n = n_a + n_v$. If atoms occupy all lattice sites, the system's total volume is given by $V = n \Omega_a$.

$$f = \frac{V - n_a \Omega_a}{n_v \Omega_a} = \frac{V - (n_a + n_v) \Omega_a + n_v \Omega_a}{n_v \Omega_a} = 1 + \frac{V - V_0}{n_v \Omega_a} \quad (8)$$

Equation (8) shows that the vacancy volume relaxation factor (f) can be determined by calculating the volume change ($V - V_0$) resulting from the presence of n_v vacancies. To explore the relationship between vacancy volume relaxation and atomic concentration, the vacancy concentration (C_v), atomic concentration (C_a), and lattice concentration (C_0) are defined as follows:

$$C_v = \frac{n_v}{V_0} \quad (9)$$

$$C_a = \frac{n_a}{V_0} \quad (10)$$

$$C_0 = \frac{n}{V_0} = \Omega_a^{-1} \quad (11)$$

Where $C_v + C_a = C_0$. In this study, C_{v0} was employed as the initial vacancy concentration, and C_{a0} represents the initial atomic vacancy concentration. Because the initial vacancy concentration is approximately $10^{-6} C_0$, we can reasonably approximate C_{a0} to be equal to C_0 .

4.2. Simulation details

We employed MD simulations executed in the large-scale atomic/molecular massively parallel simulator (LAMMPS). To adjust the vacancy concentration according to Eq. (9), we randomly removed a specific number of atoms from the current model. Before the nanoindentation test, the system's pressure in all directions was thoroughly equilibrated

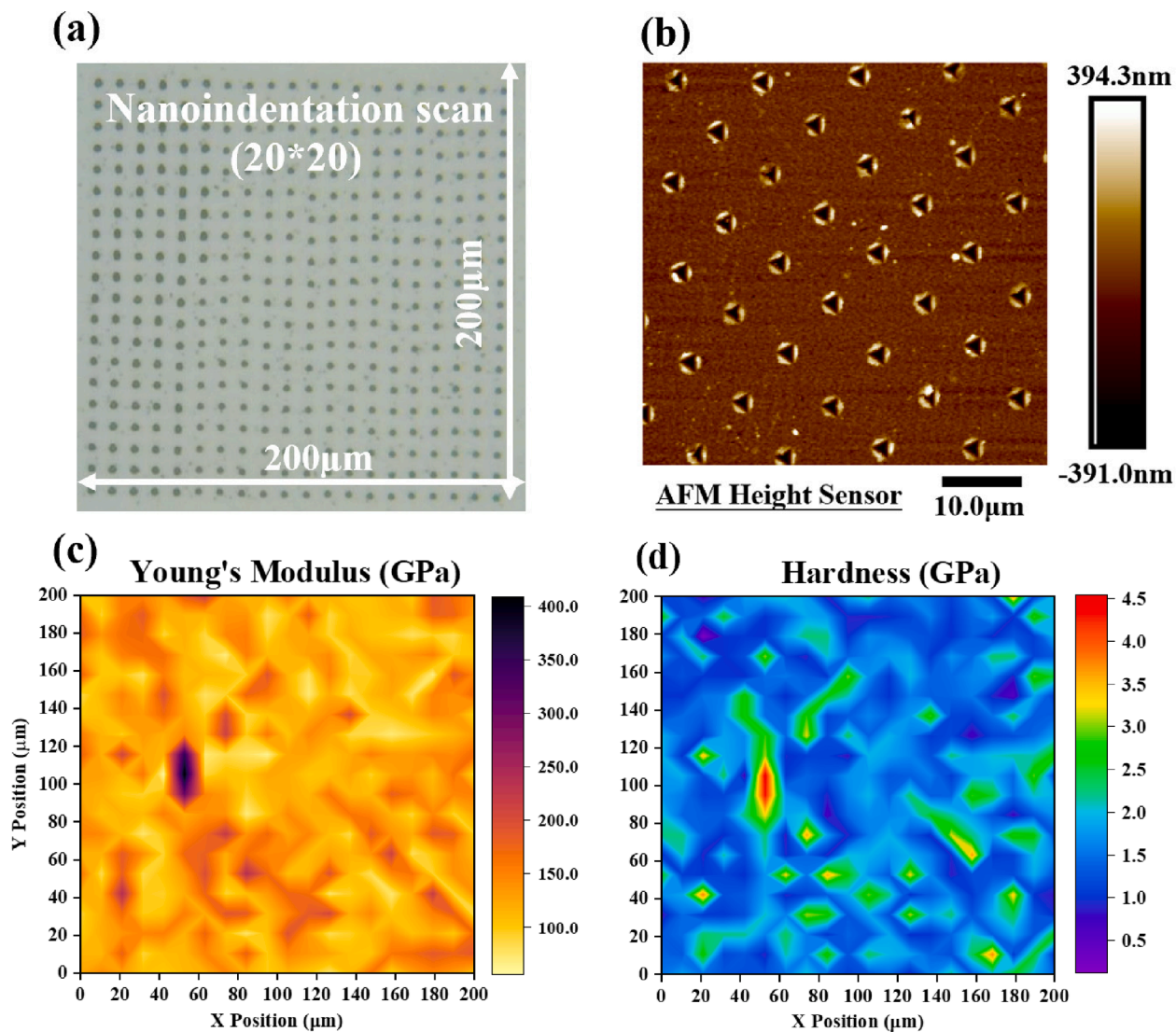


Fig. 4. (a) Morphologies of the Al interconnect after nanoindentation test; (b) topographical map of the surface scanned by AFM; and distributions of (c) Young's modulus (E) and (d) hardness (H) in the tested region.

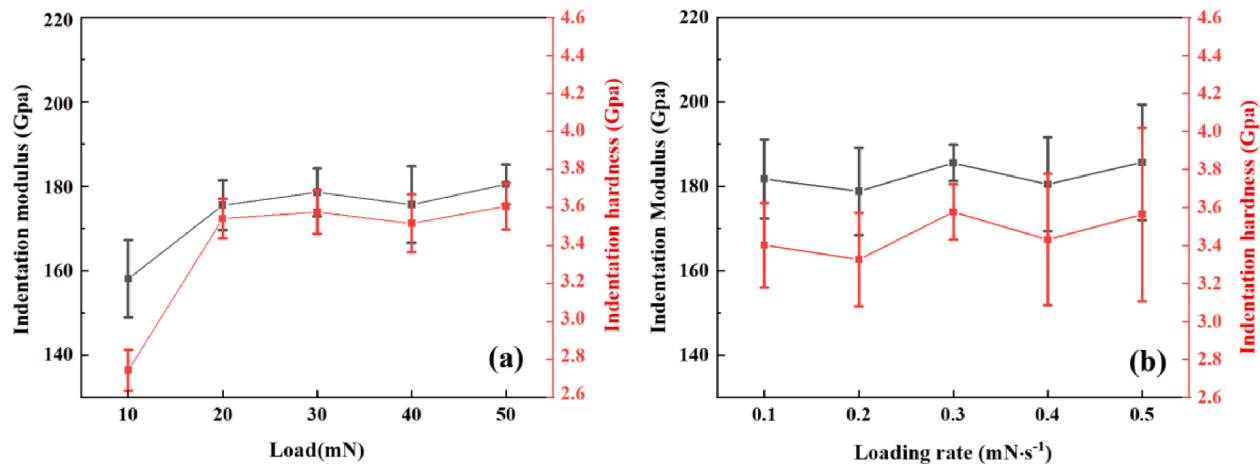


Fig. 5. Young's modulus and hardness: (a) under different indentation loads and (b) under different loading rates.

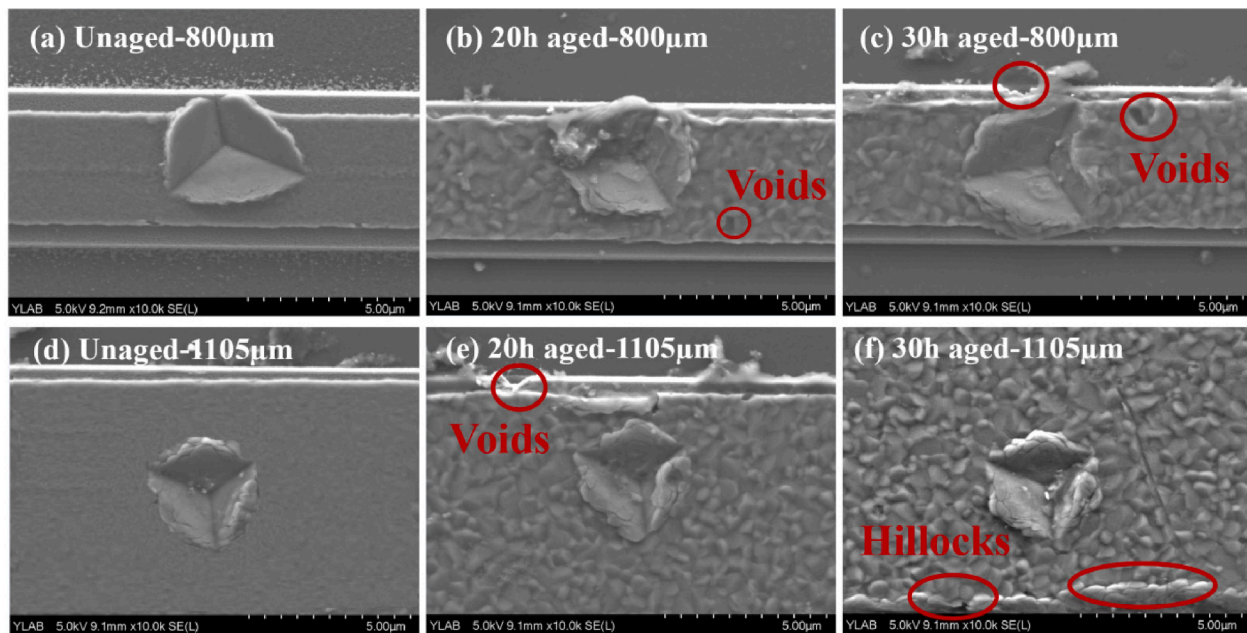


Fig. 6. SEM scans: 800-µm interconnects (a) before EM test, (b) EM test for 20 h, and (c) EM test for 30 h; 1105-µm interconnects (d) before EM test, (e) EM test for 20 h, and (f) EM test for 30 h.

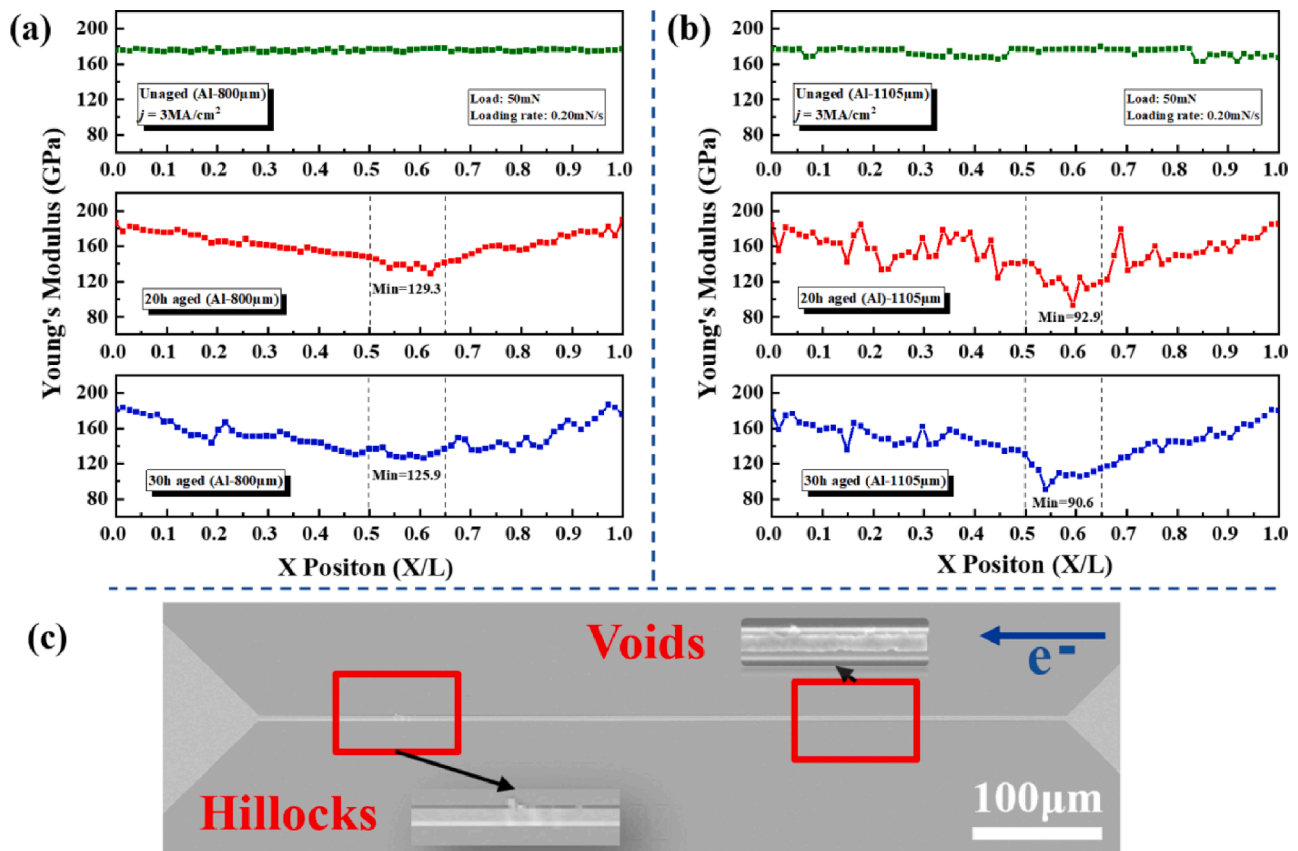


Fig. 7. Young's modulus-indentation position curves: (a) 800 µm, (b) 1105 µm, and (c) initiation region of voids and hillocks in the interconnect.

under the isothermal-isobaric ensemble (NPT). First, the loading process of Al interconnects with different indentation depths was simulated. Second, the indentation performance was simulated with models of different void concentrations. The calculation results were visualized using the open visualization tool (OVITO), and a dislocation extraction

algorithm (DXA) was employed to statistically analyze and output the types and lengths of dislocations in the model.

To simulate the nanoindentation process, we employed the classical embedded atom method (EAM) potential developed by Foiles et al. [33] to describe the interactions among Al atoms. The total energy E_{tot} can be

represented as follows [34]:

$$E_{tot} = \sum_i F_i(\theta_{h,i}) + 0.5 \sum_{i=1} \sum_{j(j^i)} q_{ij}(R_{ij}) \quad (12)$$

where $\theta_{h,i}$, $F_i(\rho)$, and $R_{ij}(R_{ij})$ are the host electron density of the i^{th} atom, the energy to embed the i^{th} atom into the background electron density ρ , and the core-core pair repulsion between i^{th} and j^{th} atoms with a distance of R_{ij} .

Fig. 8 illustrates the initial model used to study nanoindentation performance. The initial model is divided into three parts: fixed layers, thermostatic layers, and Newtonian layers. The fixed layers immobilize the model, preventing any movement during the nanoindentation process. The thermostatic layers control the system's temperature. Atomic movement and structural evolution occur in the Newtonian layers. The initial model has crystal orientations in the X, Y, and Z directions represented by [100], [010], and [001], respectively, with dimensions of $300 \times 300 \times 1400 \text{ \AA}$, comprising $\sim 1,425,000$ atoms. To simulate the generation of EM in the interconnect, we randomly removed a specific number of atoms, resulting in different void concentrations, with the void concentration corresponding to the degree of EM degradation. In this study, all simulated systems employed periodic boundaries and underwent energy minimization using the conjugate gradient algorithm (CGA). Throughout the indentation process, the temperature of the entire system was maintained at 293.15 K. The simulation time step was set to 1 fs. The temperature of the entire system was controlled using a Nosé-Hoover thermostat, and the velocity Verlet algorithm was employed to track the positions of individual atoms in the system. Subjecting the system to a 1000-ps relaxation was sufficient to bring the system to equilibrium even at high vacancy concentrations.

4.3. Influence of void concentration

In crystal plasticity theory, the total deformation gradient F can be divided into two parts: the deformation gradient F^p associated with crystal slip along the slip system, and the deformation gradient F^* corresponding to lattice distortion and rigid body rotation.

$$F = F^* F^p \quad (13)$$

The velocity gradient tensor L can be decomposed into the elastic deformation part L^* and the plastic deformation part L_p .

$$L = \dot{F}F^{-1} = L^* + L^p \quad (14)$$

$$L^* = \dot{F}^* F^{*-1} \quad (15)$$

$$L^p = \dot{F}^p F^{p-1} = \sum_{a=1}^n m^{*\alpha} \dot{\gamma}^\alpha s^{*\alpha} \quad (16)$$

Where $s^{*\alpha}$ and $m^{*\alpha}$ represent the slip direction and the normal to the slip plane of the α slip system, respectively, in the reference configuration. Equations (13) to (16) establish the connection between the macroscopic deformation of the crystal and the microscopic shear strain rate due to slip.

Define the Schmid resolved shear stress τ^α as:

$$\tau^\alpha = \tau : P^\alpha \quad (17)$$

where τ represents the Kirchhoff stress tensor,

$$P^\alpha = \frac{s^\alpha m^\alpha + m^\alpha s^\alpha}{2} \quad (18)$$

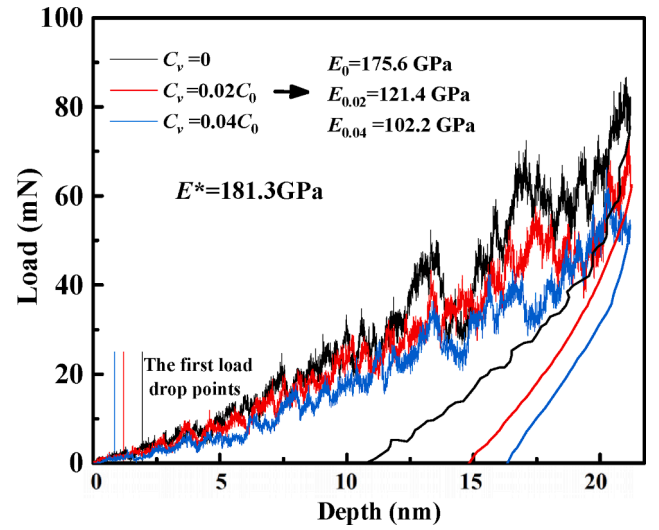


Fig. 9. P - h curves of the models with varying void concentrations.

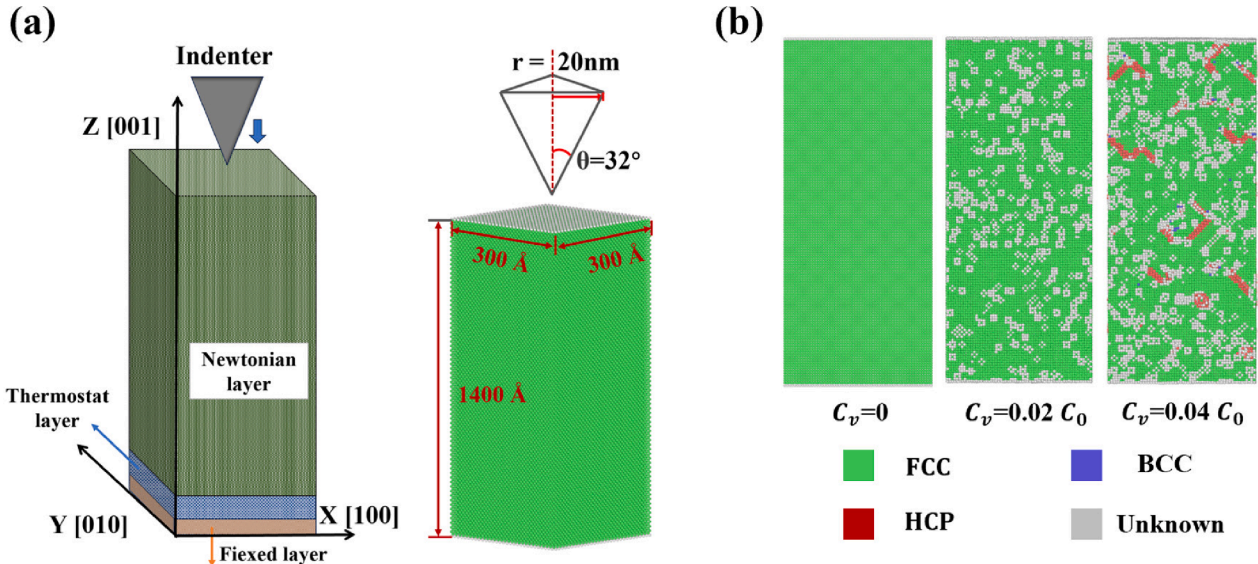


Fig. 8. (a) Simulation cell for nanoindentation of the Al interconnect and (b) lattice structure for Al, determined via polyhedral template matching at different vacancy concentrations.

At a constant rate of $v = 0.2 \text{ \AA/ps}$, the indenter was pressed into models with varying void concentrations, producing the corresponding P - h curves shown in Fig. 9. Overall, the indentation process can be divided into two main stages: elastic deformation and plastic deformation. In the initial stage of elastic deformation, the load gradually increases with the indentation depth, reflecting the behavior of elastic materials under stress. Fig. 2 shows that, at the same indentation depth, the indentation load decreased with an increase in void concentration within the model, demonstrating a pronounced Hall–Petch phenomenon [35].

The Hall–Petch phenomenon is attributed to the significant influence of internal voids on the plastic deformation behavior of the material. Voids within the crystal act as obstacles to dislocation motion, hindering slip and movement of dislocations, thus enhancing the material's yield strength. Under both experimental and simulation conditions, an increase in the applied current duration and void concentration resulted in a decreased crystal strength. This behavior aligns with the expectations dictated by the Hall–Petch relationship. The first load drop points on the P - h curve correspond to indentation depths of 1.511, 1.296, and 0.924 nm. This indicates that with an increase in cavity concentration, the plasticity of the material decreases, suggesting that void concentration variations significantly affect the material's mechanical properties during nanoindentation.

During nanoindentation, elevated stress regions are generated around the indenter as it penetrates the material. When the accumulated stress within the crystal surpasses the critical resolved shear stress, lattice distortion occurs, and this stress is released through the nucleation and glide of dislocations. Fig. 10 shows the variation in the lengths of different types of dislocations and the total dislocation length with increasing indentation depth.

At an indentation depth of 0.5 nm, Shockley partial dislocations ($1/6\langle 112 \rangle$) first appear in Al. As the indentation depth increases, various types of dislocations emerge, including complete dislocations ($1/2\langle 110 \rangle$), Hirth partial dislocations ($1/3\langle 100 \rangle$), stair-rod partial dislocations ($1/6\langle 110 \rangle$), and Frank partial dislocations ($1/3\langle 111 \rangle$). The lengths of total dislocations and the individual dislocations increase as the indentation depth increases. Among these dislocation types, Shockley partial dislocations dominate the scene in Al nanoindentation, with lengths significantly exceeding those of other dislocation types.

During the process of nanoindentation, dislocations nucleate beneath the indenter. As the penetration depth increases, dislocations spread within the matrix along the depth direction, causing significant plastic deformation of the material. Under different void concentrations, Shockley partial dislocations predominantly contribute to the total dislocation formation during the nanoindentation process, indicating

that the growth and slip of Shockley partial dislocations constitute the primary mechanism for material plastic deformation. Compared to Shockley partial dislocations, the quantities of stair-rod and Hirth partial dislocations are relatively low. This is attributed to the higher requirements for forming stair-rod and Hirth partial dislocations, which necessitate specific layer stacking conditions between two Shockley partial dislocations. Notably, the population of Frank partial dislocations remains consistently low throughout the entire nanoindentation process. This suggests that the generation and evolution of Frank's partial dislocations are comparatively challenging. The formation of Frank partial dislocations requires overcoming high energy barriers, resulting in their infrequent occurrence under actual nanoindentation conditions.

The variation in dislocation density has a significant influence on the hardening behavior of crystals. During plastic deformation of crystals, as the dislocation density increases, the interaction between dislocations strengthens, making dislocation slip more difficult and requiring an increase in stress for further movement. Specifically, the mechanisms that cause strain hardening in crystals mainly include the following forms: dislocation pile-up, cross-slip, immobilization of moving dislocations by captured dislocations, and continuous consumption of dislocations by Frank sources.

The evolution from the nucleation and glide of dislocations to the formation of independent dislocation loops is a complex process with increasing indentation depth (depicted by the black dashed circles in Fig. 11). Dislocations and stacking faults beneath the indenter continuously increase, leading to the movement of dislocations and stacking faults toward the boundaries of the model. Simultaneously, some dislocations separate from those near the indenter, forming an approximately rhombic dislocation loop, also known as a prismatic dislocation loop (PDL). Fig. 11 (a) and (b) show that when the void concentration is 0, the dislocation loop consists of Shockley partial dislocations. As the void concentration increases, the nature of the dislocation loop undergoes a transformation from Shockley partial dislocations to stair-rod partial dislocations.

With the progression of the indenter loading, dislocation accumulation becomes concentrated at the indenter contact area during the plastic deformation stage. As the applied force by the indenter continues to increase, dislocations progressively extend and propagate outward from the contact region, eventually leading to plastic deformation dominated by the slip of multiple dislocations. Subsequently, dislocations accumulate, and slip bands continuously form and merge, ultimately causing permanent damage to the substrate model during unloading.

The plastic deformation of single-crystal Al is primarily induced by

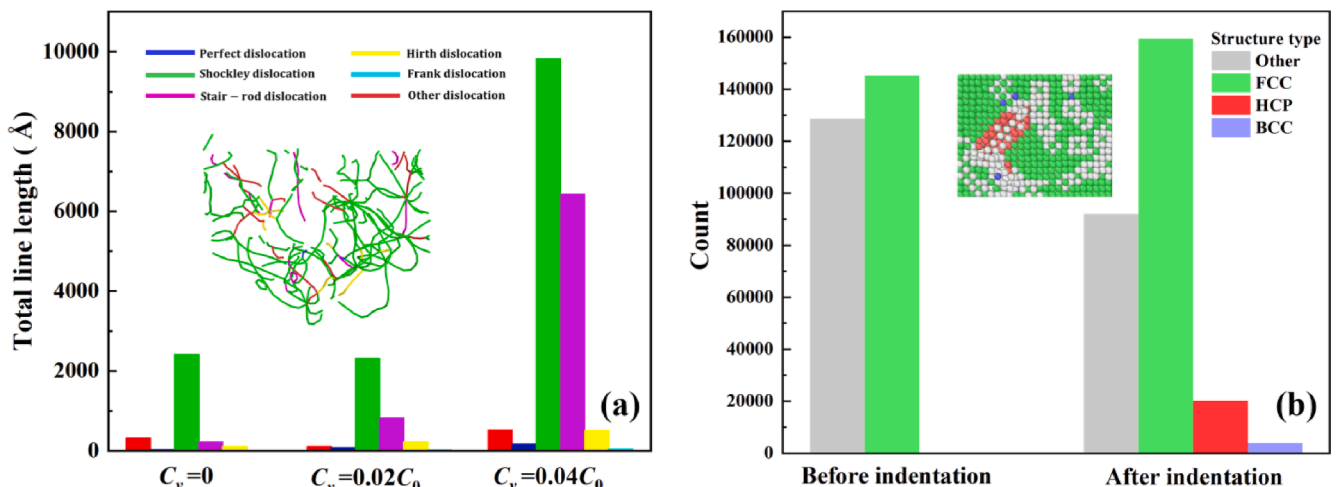


Fig. 10. (a) Dislocation histogram for the total dislocation and different types of dislocation and (b) structure type before and after indentation ($C_v = 0$).

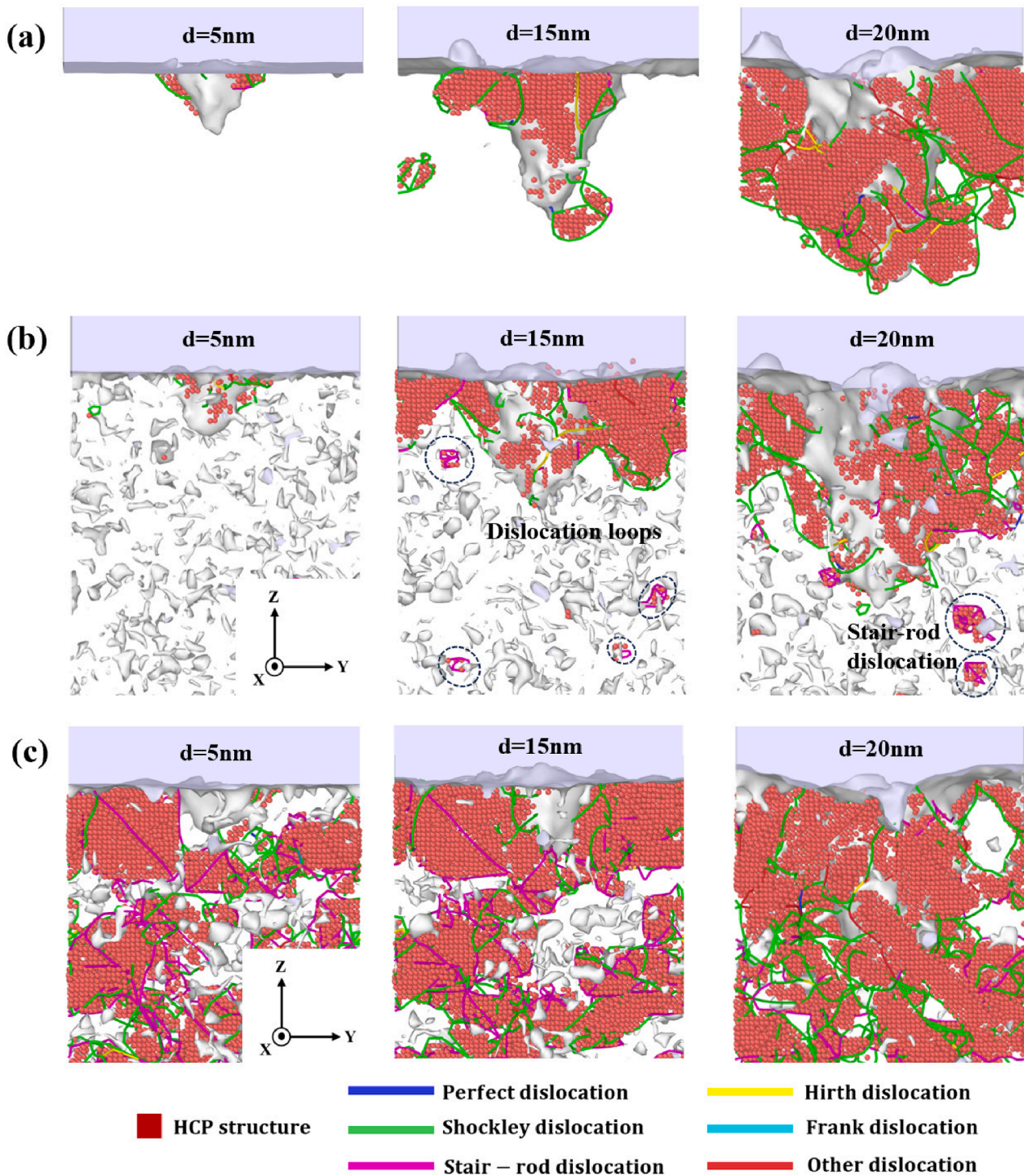


Fig. 11. Dislocation nucleation and evolution: (a) $C_v = 0$, (b) $C_v = 0.02C_0$, and (c) $C_v = 0.04C_0$.

generating multiple slip bands [26]. During the nanoindentation process, the plastic deformation of single-crystal Al is primarily caused by the generation of multiple slip bands. At the peak load, corresponding dislocation slip bands form within the grains around the contact region. With an increase in void concentration, the dislocation slip bands within the grains become more pronounced, and the number of slip bands increases, damaging adjacent grain boundaries. Compared to defect-free single-crystal Al, the nanoindentation process with voids on the nano-aluminum substrate model leads to more extensive and significant plastic deformation. Unlike plastic deformation primarily occurring at

the contact area in single-crystal Al, voids result in more prominent plastic deformation at grain boundaries and within the grains. This includes the accumulation of dislocations with HCP structures at grain boundaries and the forming of slip bands in adjacent grains. The extent of structural plastic deformation increases with the void concentration, especially under the condition of $C_v = 0.04$. Multiple dislocation loops can be observed forming within the simulation units. These dislocation loops are permanent markers of plastic deformation released into the system (Fig. 12).

The evolution of stacking faults and dislocations reveals a

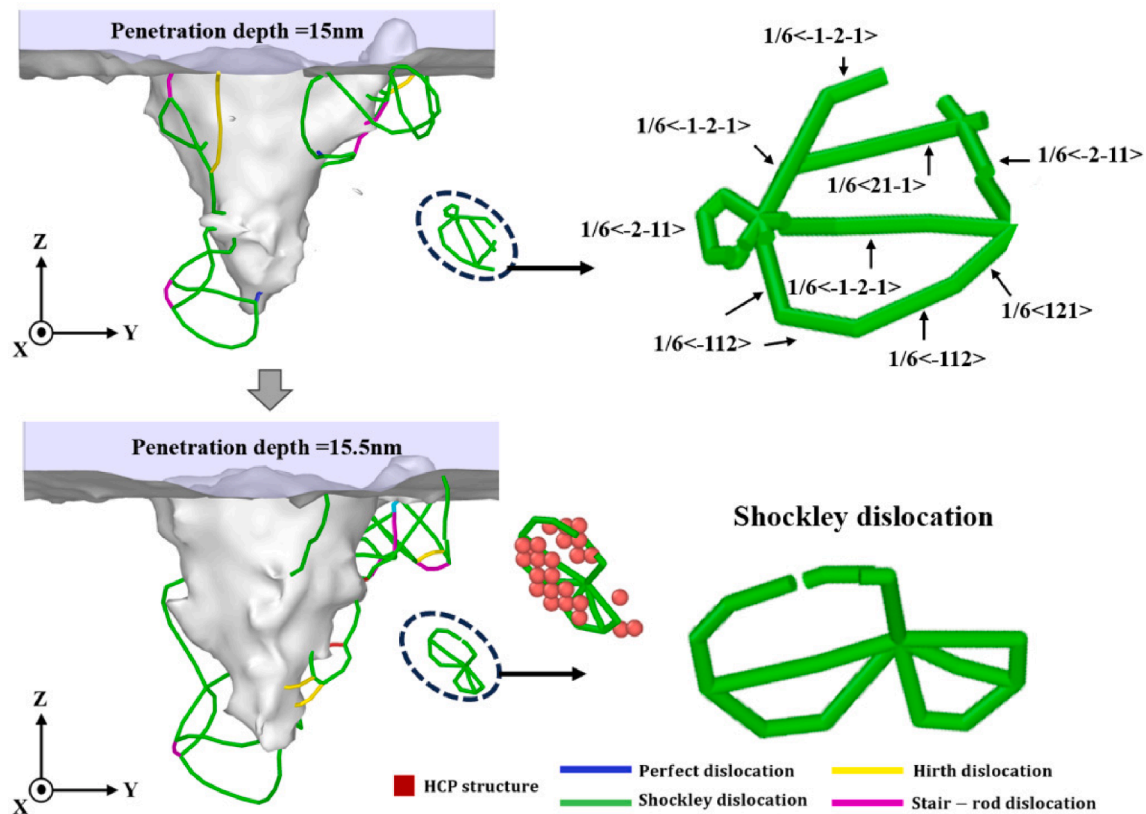


Fig. 12. Evolution of dislocation loops.

considerable increase in defect structures with increasing indentation depth. Stacking faults, various dislocations, and dislocation loops continuously nucleate and grow within the model. The overall deformation analysis indicates that the competition between material softening induced by plastic yield and strain hardening caused by stair-rod and Hirth partial dislocations is responsible for the sawtooth-like fluctuations shown in the load–displacement curve (Fig. 9).

Based on a series of nanoindentation experiments and molecular dynamics simulations, it can be observed that in FCC metals, an increase in void concentration leads to an increase in the number and density of dislocations within the structure, resulting in a decrease in material strength. Plastic strain bursts are comprised of numerous dislocation slip events [36]. Dislocation motion is governed by phonon drag, and the situation becomes more complex due to the strong influence of various collective phenomena associated with elastic interactions between dislocations. Within a certain range of dislocation densities, an increase in dislocation density results in a decreasing trend in material strength [37].

5. Conclusions

In this study, we employed a combination of nanoindentation experiments and MD simulations for a multiscale analysis of the mechanical properties of Al interconnects subjected to varying degrees of EM. Our investigation involved a microscopic analysis of how EM affects the mechanical performance of the interconnect and examining the relationship between mechanical properties and void formation. EM involves the flow of metal atoms, and we scrutinized its effects on voids and their potential contributions to dislocation nucleation, particularly in the formation of dislocation loops at the atomic scale.

The results are as follows. (1) The Young's modulus and hardness of the Al interconnect gradually increase and stabilize after 20 mN. Still, within a specific range, the influence of the loading rate on the

indentation depth and mechanical properties is relatively small. (2) There is a correlation between the location where EM-induced voids initiate and the region where Young's modulus of the interconnect decreases. The formation of voids caused by EM directly affects the mechanical properties of the material, especially the decrease in Young's modulus. (3) EM-induced voids affect the nucleation and formation of dislocations. With the increase in void concentration and indentation depth, the generation and slip of dislocations gradually increase and the material strength gradually decreases.

Through this multiscale approach, we gained a deeper understanding of the microscopic effects of EM on the mechanical properties of materials and unraveled the intricate interplay between EM and void formation. This comprehensive analysis expands our knowledge of the behavior of interconnect materials under EM conditions, providing a scientific basis for designing and optimizing electronic devices. Moreover, as the actual Al interconnection wires are always with polycrystal and grain boundaries, in the future, we will consider the effects of polycrystal and grain boundaries, dislocations, and other defects in the MD simulations, providing a more comprehensive understanding of mechanical failure at grain level, that can contribute to the overall mechanical performance evaluation on actual Al interconnection wires.

CRediT authorship contribution statement

Shuo Feng: Writing – original draft, Visualization, Investigation, Formal analysis, Data curation. **Leiming Du:** Writing – review & editing, Validation. **Zhen Cui:** Resources, Investigation. **Xi Zhu:** Writing – review & editing. **Xuejun Fan:** Supervision, Conceptualization. **Guoqi Zhang:** Supervision. **Jiajie Fan:** Validation, Supervision, Resources, Project administration, Funding acquisition, Conceptualization.

Declaration of competing interest

The authors declare that they have no known competing financial interests or personal relationships that could have appeared to influence the work reported in this paper.

Data availability

Data will be made available on request.

Acknowledgments

This work was partially supported by National Natural Science Foundation of China (No. 52275559), Shanghai Pujiang Program (No. 2021PJD002) and Shanghai Science and Technology Development Funds (No. 19DZ2253400).

References

- [1] Y. Yang, L. Dorn-Gomba, R. Rodriguez, C. Mak, A. Emadi, Automotive power module packaging: current status and future trends, *IEEE Access* 8 (2020) 160126–160144.
- [2] H. Ceric, H. Zahedmanesh, K. Croes, Analysis of electromigration failure of nano-interconnects through a combination of modeling and experimental methods, *Microelectronics Reliability* 100–101 (2019/09/01/ 2019) 113362.
- [3] Y. Wang, B. Li, Y. Zhifeng, Y. Yao, Interfacial fracture caused by electromigration at copper interconnects, *Journal of Electronic Packaging* 146 (1) (2023).
- [4] C.-L. Liang, et al., Athermal and thermal coupling electromigration effects on the microstructure and failure mechanism in advanced fine-pitch Cu interconnects under extremely high current density, *Materials Chemistry and Physics* 256 (2020/12/01/ 2020.) 123680.
- [5] F. Wolff, D. Weyer, C. Papachristou, S. Clay, Design for reliability: tradeoffs between lifetime and performance due to electromigration, *Microelectronics Reliability* 117 (2021/02/01/ 2021.) 114025.
- [6] I.A. Blech, Electromigration in thin aluminum films on titanium nitride, *Journal of Applied Physics* 47 (4) (2008) 1203–1208.
- [7] C. Basaran, Unified mechanics of metals under high electrical current density: electromigration and thermomigration, in: *Introduction to unified mechanics theory with applications*, Springer International Publishing, Cham, 2022, pp. 427–458.
- [8] K. Sasagawa, M. Hasegawa, M. Saka, H. Abé, Atomic flux divergence in bamboo line for predicting initial formation of voids and hillocks, *Theoretical and Applied Fracture Mechanics* 33 (1) (2000/02/01/ 2000.) 67–72.
- [9] Y. Zhang, Y. Liu, L. Liang, X. Fan, The effect of atomic density gradient in electromigration, *International Journal of Materials and Structural Integrity* 6 (1) (2012/01/01 2012.) 36–53.
- [10] Z. Cui, X. Fan, Y. Zhang, S. Vollebregt, J. Fan, G. Zhang, Coupling model of electromigration and experimental verification – Part I: effect of atomic concentration gradient, *Journal of the Mechanics and Physics of Solids* 174 (2023/05/01/ 2023.) 105257.
- [11] M.E. Sarychev, Y.V. Zhitnikov, L. Borucki, C.L. Liu, T.M. Makhviladze, A new, general model for mechanical stress evolution during electromigration, *Thin Solid Films* 365 (2) (2000) 211–218.
- [12] I.A. Blech, C. Herring, Stress generation by electromigration, *Applied Physics Letters* 29 (3) (1976) 131–133.
- [13] M.A. Korhonen, P. Borgesen, K.N. Tu, C.Y. Li, Stress evolution due to electromigration in confined metal lines, *Journal of Applied Physics* 73 (8) (1993) 3790–3799.
- [14] A.G. Custodio, K.J. Lindquist, M. Tolentino, C. Aranas, G.C. Saha, Investigating the nanoscale hardness/strength properties of high-entropy alloy particles using the nanoindentation technique, *Journal of Alloys and Metallurgical Systems* 4 (2023/12/01/ 2023.) 100043.
- [15] D.-Q. Doan, T.-H. Fang, T.-H. Chen, Interfacial and mechanical characteristics of TiN/Al composites under nanoindentation, *International Journal of Solids and Structures* vol. 226–227 (2021/09/01/ 2021.) 111083.
- [16] Z. Hu, Chapter 6 - Characterization of Materials, Nanomaterials, and Thin Films by Nanoindentation, in: S. Thomas, R. Thomas, A.K. Zachariah, R.K. Mishra (Eds.), *Microscopy Methods in Nanomaterials Characterization*, Elsevier, 2017, pp. 165–239.
- [17] E.S. Puchi-Cabrera, E. Rossi, G. Sansonetti, M. Sebastiani, E. Bemporad, Machine learning aided nanoindentation: a review of the current state and future perspectives, *Current Opinion in Solid State and Materials Science* 27 (4) (2023/08/01/ 2023.) 101091.
- [18] S. Mojumder, M. Mahboob, M. Motalab, Atomistic and finite element study of nanoindentation in pure aluminum, *Materials Today Communications* 23 (2020/06/01/ 2020.) 100798.
- [19] F. Shuang, P. Xiao, Y. Bai, Efficient and reliable nanoindentation simulation by dislocation loop erasing method, *Acta Mechanica Solida Sinica* 33 (5) (2020/10/01 2020.) 586–599.
- [20] H.-T. Luu, S.-L. Dang, T.-V. Hoang, N. Gunkelmann, Molecular dynamics simulation of nanoindentation in Al and Fe: On the influence of system characteristics, *Applied Surface Science* 551 (2021) 149221.
- [21] C. Huang, et al., Molecular dynamics simulation of BCC Ta with coherent twin boundaries under nanoindentation, *Materials Science and Engineering: A* 700 (2017/07/17/ 2017.) 609–616.
- [22] Y. Gao, C.J. Ruestes, D.R. Tramontina, H.M. Urbassek, Comparative simulation study of the structure of the plastic zone produced by nanoindentation, *Journal of the Mechanics and Physics of Solids* 75 (2015/02/01/ 2015.) 58–75.
- [23] Q. Liu, L. Deng, X. Wang, J. Li, Formation of stacking fault tetrahedron in single-crystal Cu during nanoindentation investigated by molecular dynamics, *Computational Materials Science* 131 (2017/04/15/ 2017.) 44–47.
- [24] Y. Wang, M. Minhaj, X. Wang, J. Shi, Deformation behaviors and inverse Hall-Petch effect in nanoindentation of silicon: an atomistic simulation study with experimental validation, *Journal of Manufacturing Processes* 74 (Feb 2022) 319–331.
- [25] S. Jiao, et al., Atomistic insights into the prismatic dislocation loop on Al (1 0 0) during nanoindentation investigated by molecular dynamics, *Computational Materials Science* 143 (2018/02/15/ 2018.) 384–390.
- [26] A. Kumar Panda, R. Divakar, A. Singh, R. Thirumurugesan, P. Parameswaran, Molecular dynamics studies on formation of stacking fault tetrahedra in FCC metals, *Computational Materials Science* 186 (2021/01/01/ 2021.) 110017.
- [27] Z. Cui, X. Fan, G. Zhang, Molecular dynamic study for concentration-dependent volume relaxation of vacancy, *Microelectronics Reliability* vol. 120. 114127 (2021) 2021/05/01.
- [28] W.C. Oliver, G.M. Pharr, An improved technique for determining hardness and elastic modulus using load and displacement sensing indentation experiments, *Journal of Materials Research* 7 (6) (1992/06/01 1992.) 1564–1583.
- [29] M. Machado, P. Moreira, P. Flores, H. Lankarani, Compliant contact force models in multibody dynamics: evolution of the Hertz contact theory, *Mechanism and Machine Theory* 53 (07/01 2012) pp. 99–121.
- [30] M.B. Kelly, S. Niverty, N. Chawla, Electromigration in Bi-crystal pure Sn solder joints: elucidating the role of grain orientation, *Journal of Alloys and Compounds* 818 (2020/03/25/ 2020.) 152918.
- [31] P.-T. Lee, et al., Synchrotron X-ray study of electromigration, whisker growth, and residual strain evolution in a Sn Blech structure, *Scripta Materialia* 214 (2022/06/01/ 2022.) 114682.
- [32] Y.-H. Liao, C.-H. Chen, C.-L. Liang, K.-L. Lin, A.T. Wu, A comprehensive study of electromigration in pure Sn: effects on crystallinity, microstructure, and electrical property, *Acta Materialia* 200 (2020/11/01/ 2020.) 200–210.
- [33] S.M. Foiles, M.I. Baskes, M.S. Daw, Embedded-atom-method functions for the fcc metals Cu, Ag, Au, Ni, Pd, Pt, and their alloys, *Physical Review B* 33 (12) (06/15/ 1986) pp. 7983–7991.
- [34] M.S. Daw, S.M. Foiles, M.I. Baskes, The embedded-atom method: a review of theory and applications, *Materials Science Reports* 9 (7) (1993/03/01/ 1993.) 251–310.
- [35] S. Pal, K.V. Reddy, C. Deng, Improving thermal stability and Hall-Petch breakdown relationship in nanocrystalline Cu: A molecular dynamics simulation study, *Materials Letters* 324 (2022) 132821.
- [36] J. Alcalá, J. Očenásek, J. Varillas, J.A. El-Awady, J.M. Wheeler, J. Michler, Statistics of dislocation avalanches in FCC and BCC metals: dislocation mechanisms and mean swept distances across microsample sizes and temperatures, *Scientific Reports* 10 (1) (2020/11/04 2020.) 19024.
- [37] H. Fan, Q. Wang, J.A. El-Awady, D. Raabe, M. Zaiser, Strain rate dependency of dislocation plasticity, *Nature Communications* 12 (1) (2021/03/23 2021.) 1845.